Int j simul model 23 (2024) 1, 184-195
Original scientific paper

FAULT PREDICTION IN HIGH-EFFICIENCY PETROLEUM MACHINERY PRODUCTION

He, D. X.
College of Mechanical Engineering, Yangtze University, Jingzhou 434000, China
E-Mail: 18905468956@163.com

Abstract
This paper introduces a fault diagnosis and prediction framework for petroleum machinery production systems, addressing the need for more efficient and reliable fault handling in the face of complex signals. Utilizing the Complete Ensemble Empirical Mode Decomposition (CEEMD) and permutation entropy, it extracts signal features to analyse system dynamics. An Adaptive Variational Mode Decomposition (VMD) and optimized Extreme Learning Machine (ELM) simulation model enhances diagnostic accuracy through signal processing and fast learning capabilities. This approach not only elevates fault diagnosis precision but also supports the maintenance and health management of petroleum machinery systems, offering significant theoretical and practical benefits.
(Received in October 2023, accepted in February 2024. This paper was with the author 3 weeks for 1 revision.)

Key Words: Petroleum Machinery Production Systems, Fault Prediction, Signal Processing, CEEMD, VMD, ELM

1. INTRODUCTION

As global energy demand grows, petroleum's role in the energy sector is increasingly crucial, necessitating efficient petroleum machinery production systems for stable energy supply, enhanced oil extraction, and reduced costs [1-3]. However, these systems face risks of degradation and faults due to extreme conditions and complex operations [4-6], highlighting the importance of research on their performance and fault prediction to ensure safety and reliability [7, 8].

Advancements in information technology and intelligent algorithms have made the improvement of monitoring and maintenance for petroleum machinery a key research area [9]. Accurate data analysis and fault prediction models enable early warnings, facilitating timely interventions that ensure production continuity and safety, reduce downtime, and decrease maintenance costs, boosting industry competitiveness [10-13].

Traditional methods struggle with the complex, nonlinear, and non-stationary signals from petroleum machinery, limiting fault diagnosis accuracy due to inadequate signal decomposition and feature extraction [14-16]. Furthermore, fault diversity and environmental noise complicate model construction, affecting model generalization and reliability [17].

This study introduces a new approach for simulating and analysing petroleum machinery signals using CEEMD and permutation entropy, capturing signal features and dynamics. It also develops a fault diagnosis model combining Adaptive VMD and optimized ELM, leveraging their strengths in signal processing and fast learning to enhance diagnostic accuracy. This research offers valuable theoretical and technical insights for petroleum machinery management and presents a novel predictive tool with broad academic and practical implications.

2. PETROLEUM MACHINERY VIBRATION SIGNAL ANALYSIS

This paper utilizes CEEMD and permutation entropy to analyse vibration signals from petroleum machinery, aiding efficient operation in harsh environments. CEEMD breaks down

signals into Intrinsic Mode Functions (IMFs) to unveil dynamic characteristics and analyse fault features within specific frequencies. Permutation entropy then quantifies the complexity of these IMFs, with high values indicating potential faults. This combination enhances traditional signal analysis, allowing precise identification of dynamic changes and faults in the machinery. This method improves fault diagnosis and boosts the performance and economy of petroleum production systems.

2.1 CEEMD

Initially, a certain number of white noise sequences are added to the original vibration signal $t(v)$. The introduction of white noise helps to avoid mode mixing and provides a stabilizing effect during the decomposition process. Assuming the white noise sequence added for the u^{th} $(1, 2, .., U)$ time is represented by $n^u(v)$, the u^{th} sequence can be represented as $t^u(v) = t(v) + n^u(v)$. The j^{th} modal component produced by the decomposition through two methods is represented by $Rj(.)$ and $D_{UL,j}$. Fig. 1 presents the flowchart of the CEEMD.

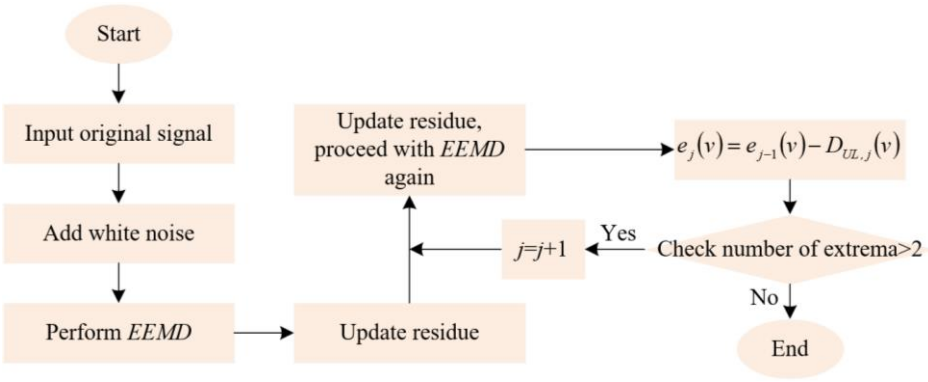

Figure 1: Flowchart of CEEMD.

Furthermore, classical Empirical Mode Decomposition (EMD) is performed on each signal containing white noise. EMD is a fully adaptive process that does not rely on fixed basis functions but extracts various IMFs directly from the data, starting from the highest frequency to the lowest frequency. These IMFs are essential components of the signal, composed of simple oscillatory modes, and each IMF should satisfy two conditions: the number of extrema and the number of zero-crossings must either be equal or differ by at most one throughout the entire dataset; at any point, the mean value of the envelope defined by the local maxima and the envelope defined by the local minima should be zero. If the signal sequence $t(v) + \gamma_0 n^u(v)$ is decomposed U times. The expression for the first modal component extracted by the EMD method is given by:

$$D_{UL,1}(v) = \frac{1}{U}\sum_{u=1}^{U} D^{u}_{U4L,1}(v) = \overline{D_{UL,1}}(v) \tag{1}$$

The expression for the first residual signal corresponding to the first decomposition is given by:

$$e_1(v) = t(v) - D_{UL,1}(v) \tag{2}$$

Continue to calculate the second modal component, expressed as:

$$D_{UL,2}(v) = \frac{1}{U}\sum_{u=1}^{U} R_1\left(e_1(v)\right) + \gamma_1 R_1\left(n^u(v)\right) \tag{3}$$

Repeat the above steps several times, each calculation process is consistent with the described process, adding different sequences of white noise to the original signal each time,

then performing EMD, and extracting the corresponding IMFs. The expression for calculating the j+1 [th] modal component is given by:

$$e_j(v) = e_{j-1}(v) - D_{UL,j}(v) \tag{4}$$

$$D_{UL,j+1}(v) = \frac{1}{U}\sum_{u=1}^{U} R_1\left(e_j(v)\right) + \gamma_j R_j\left(n^u(v)\right) \tag{5}$$

For each intrinsic mode, the IMFs of the same mode extracted from all iterations are averaged to obtain the final IMFs. This process removes the influence of white noise, as the effects of white noise will cancel each other out over multiple iterations. After extracting all the IMFs, the residual signal is calculated, which contains the trend part of the original signal that has not been decomposed. The expression for the residual signal is:

$$E(v) = t(v) - \sum_{j=1}^{J} D_{UL,j} \tag{6}$$

Assuming the original signal is represented by $t(v)$, and is decomposed into $\Sigma^{J}_{j=1}D_{IL,j}$ and $E(v)$, then we have:

$$t(v) = E(v) + \sum_{j=1}^{J} D_{UL,j} \tag{7}$$

2.2 Permutation entropy

In the context of CEEMD steps for vibration signals of high-efficiency petroleum machinery production systems, when combined with permutation entropy, it involves the reconstruction of time series in phase space, permutation, acquisition of symbolic sequences, and calculation of permutation entropy. The following are the detailed steps combining these aspects:

First, starting with the time series of vibration signals from petroleum machinery, the multiple IMFs obtained by decomposing the signal with CEEMD are used for phase space reconstruction, thus forming a reconstructed vector matrix. This process can reveal the dynamic structure and potential regularities of the original time series. Let the time series be represented by $\{a(u), u = 1, 2, .., v\}$, the embedding dimension by l, and the delay time by π, with $k = 1, 2, ...,$ J, $J = v-(l-1)\pi$, the formed reconstructed vector matrix is as follows:

$$\begin{bmatrix} a(1) & a(1+\pi) & \cdots & a(1+(l-1)\pi) \\ \vdots & \vdots & & \vdots \\ a(k) & a(k+\pi) & \cdots & a(k+(l-1)\pi) \\ \vdots & \vdots & & \vdots \\ a(J) & a(J+\pi) & \cdots & a(J+(l-1)\pi) \end{bmatrix} \tag{8}$$

For each vector reconstructed in phase space, sort its elements by numerical value. This does not change the order of the data itself but sorts the positions corresponding to these elements, obtaining a new index sequence that reflects the relative magnitude relationships of the original data. Let the k^{th} reconstructed vector in the reconstruction matrix be represented by $a(k)$, $a(k+\pi)$, .., $a[k+(l-1)\pi]$, the new index sequence satisfies:

$$a\left[u+(k_1-1)\pi\right] \le a\left[u+(k_2-1)\pi\right] \le \cdots \le a\left[u+(k_l-1)\pi\right] \tag{9}$$

If there are equal values in the reconstructed components, then there is:

$$a\left[u+(k_1-1)\pi\right] < a\left[u+(k_2-1)\pi\right] \tag{10}$$

Based on the sorted index sequence, form a symbolic sequence. In the calculation of permutation entropy, each symbol in the sequence actually represents the permutation pattern of a local sequence in the original data. These symbolic sequences essentially characterize the intrinsic patterns and structural features of the original time series, providing a basis for subsequent permutation entropy calculations. The generated symbolic sequence is:

$$T(m)=(k_1,k_2,...,k_l),m=1,2,...,j,\ \text{and}\ j\le l! \tag{11}$$

The calculation of permutation entropy depends on the frequency of occurrence of different symbolic sequences. Count the number of times each different symbolic sequence appears in the entire time series and calculate its occurrence probability. Using these probability values, the permutation entropy can be calculated. The higher the value of permutation entropy, the higher the complexity and unpredictability of the time series; conversely, a low value of permutation entropy indicates higher regularity and predictability of the time series. If the reconstruction matrix has l dimensions, then there are $l!$ different symbolic sequences. Assuming one of the $l!$ symbolic sequences is represented by $T(m)$, and the probabilities of each symbolic sequence appearing are represented by $O_1, O_2, ..., O_j$, then the formula for calculating the permutation entropy of j different symbolic sequences of time series $a(u)$ is given by:

$$G_{OR}(l)=-\sum_{k=1}^{j}O_k\ln O_k \tag{12}$$

Through the above steps, the IMFs obtained from CEEMD can be further analysed using permutation entropy to assess the complexity of each IMF, thereby providing deeper insights in the performance analysis and fault prediction simulation study of high-efficiency petroleum machinery production systems. Such a method helps identify potential fault modes and provide early warnings.

3. FAULT DIAGNOSIS MODEL FOR EFFICIENT PETROLEUM MACHINERY

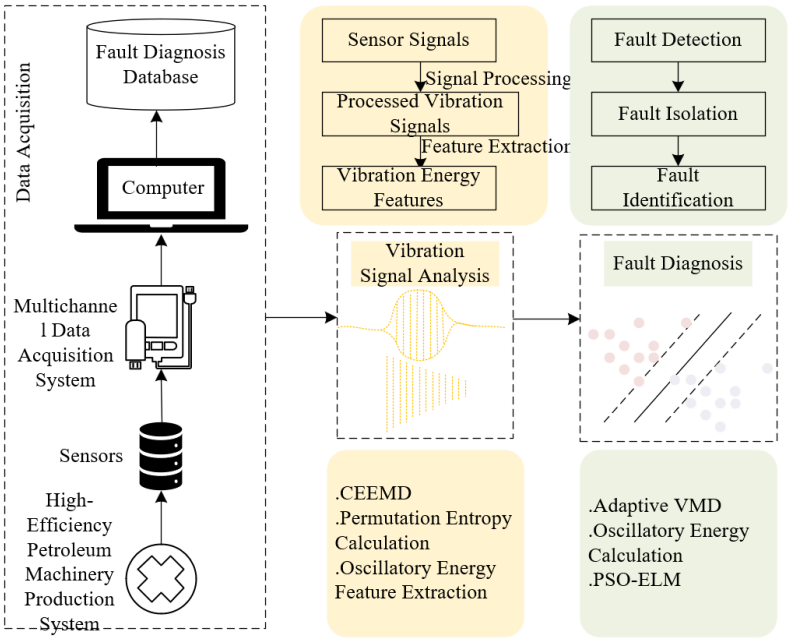

Figure 2: Fault diagnosis scheme for high-efficiency petroleum machinery production systems.

This study develops a fault diagnosis model for petroleum machinery using Adaptive VMD and optimized ELM to improve safety and economic efficiency. The model processes complex

signals and accelerates fault prediction, reducing production risks and costs. This approach meets the needs of modern petroleum machinery management and maintenance. Fig. 2 shows the model's fault diagnosis scheme.

Since petroleum machinery vibration signals often contain multiple frequency components and are affected by various noises, a fixed penalty factor may not be suitable for all situations, leading to modal overlap or insufficient decomposition accuracy. An adaptive penalty factor can dynamically adjust according to the characteristics of the signal, optimizing the accuracy and stability of the decomposition, thereby more accurately extracting signal features, improving the accuracy of fault diagnosis, and the performance of the prediction model. Specifically, this paper introduces spectral mutual correlation degree in the proposed adaptive VMD algorithm to quantify the overlap between adjacent decomposition modes. Through the quantification of the spectral mutual correlation degree, the algorithm can automatically adjust the penalty factor, making the decomposed modes as separated as possible in the frequency domain, reducing modal overlap, and ensuring the purity and reliability of the decomposition results. Suppose the Fourier transform of a specific signal or time series is represented by $D(.)$, the dot product of $D(i_u)$ and $D(i_k)$ is represented by $D(i_u)\times D(i_k)$, the sum of all elements in a one-dimensional array is represented by $\Sigma(.)$, and the sum of all $\Sigma D(i_u)\times D(i_k)$ $(u \neq k)$ is represented by $\Sigma^J_{u=1}\ \Sigma^J_{k=1}(\Sigma D(i_u)\times D(i_k)\ (u \neq k))$, the expression for the spectral mutual correlation degree is:

$$TOZ = \frac{\sum_{u=1}^{J}\sum_{k=1}^{K}\left(\sum D(i_u)\cdot D(i_k)\right)}{\sum\left(D(a)\right)^2}(u \neq k) \tag{13}$$

The approach to selecting the optimal penalty factor in the proposed adaptive VMD algorithm using the spectral mutual correlation degree is: first, set the number of modes, then further decompose each candidate penalty factor β, perform a Fourier transform on the decomposed modes to calculate the spectral mutual correlation degree. Then, average the spectral mutual correlation degrees for all candidate penalty factors β, with the average value represented by TOZ_{AV}. Finally, the penalty factor closest to the average value is chosen as the optimal value, represented by β_{HE}.

Vibration signals contain rich information about the mechanical state, and accurately extracting this information as fault features can effectively diagnose and predict faults. According to the efficient vibration signal simulation results of the petroleum machinery production system obtained in the previous section based on CEEMD and permutation entropy, the elements of the efficient petroleum machinery production system vibration signal are represented by $a^{-}a(s) = (a_1, a_2, ..., a_V)$, its energy is further obtained as R_0, and this oscillatory energy is taken as the fault feature. The vibration signal element satisfies the following formula:

$$\int_{-\infty}^{+\infty} |a(s)|^2 < \infty \tag{14}$$

The calculation formula for R_0 is:

$$R_p = \frac{1}{V}\sum_{u=1}^{V} |a_u|^2 \tag{15}$$

Assuming the initial state of the efficient petroleum machinery production system vibration signal is 0, using oscillatory energy as the fault feature, then the expression for oscillatory energy is:

$$R = \frac{1}{V}\sum_{u=1}^{V} |a_u - a_1|^2 \tag{16}$$

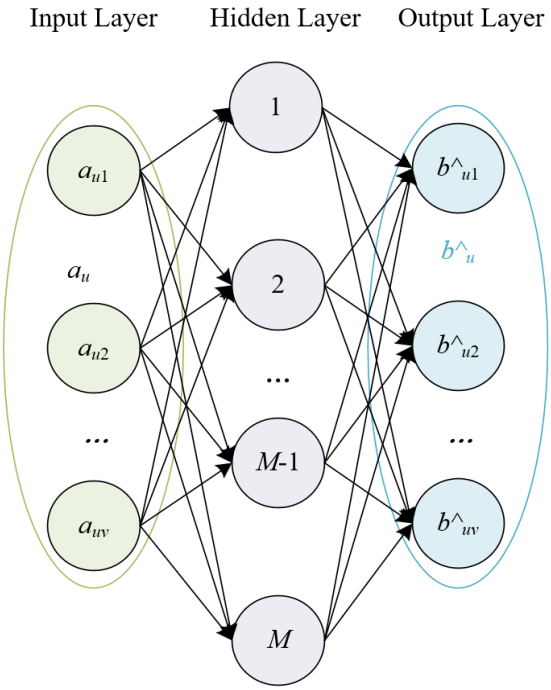

Figure 3: Structure of the Classic ELM.

In the context of performance analysis and fault prediction for high-efficiency petroleum machinery production systems, ensuring the prediction model has high accuracy and robustness is crucial, as this directly relates to the system's stable operation and maintenance costs. Fig. 3 presents the structure of the classic ELM. Because the optimized ELM has randomness in determining network parameters, which may lead to instability in the network's generalization ability and learning performance. Therefore, this paper employs the Particle Swarm Optimization (PSO) algorithm to optimize the weights and bias parameters of the ELM to enhance the accuracy and reliability of the fault diagnosis model, meeting the high demands for fault prediction accuracy and stability in the practical application of high-efficiency petroleum machinery production systems.

Initialize a group of particles, i.e., randomly generate a series of weights and biases for the ELM network. Then, use the ELM network to learn the performance data of the petroleum machinery system and evaluate the performance of each particle (i.e., each set of weights and biases) using a validation set. Based on these performance evaluations, update the particle's individual historical best position *pbest* and the group's global historical best position *gbest*. Subsequently, adjust each particle's velocity and position according to the rules of the PSO algorithm, based on *pbest* and *gbest* as well as the particle's current velocity, i.e., adjusting the weights and biases of the ELM network. Assuming the current velocity and the velocity after the next update are represented by N^j and N^{j+1}, and the current position and the position after the next update are represented by A^j and A^{j+1}, the individual learning rate and the group learning rate are represented by z_1 and z_2, e_1 and e_2 are randomly generated, the individual best value and the group best value are represented by O_{BE} and H_{BE}. The inertia factor is represented by μ. The formulas for updating velocity and position are as follows:

$$N_{ID}^{j+1} = \mu N_{ID}^{j} + z_1 e_1 \left(O_{BE}^{j} - A_{ID}^{j} \right) + z_2 e_2 \left(H_{BE}^{j} - A_{ID}^{j} \right) \tag{17}$$

$$A_{ID}^{j+1} = A_{ID}^{j} + N_{ID}^{j+1} \tag{18}$$

Assuming the maximum number of iterations is represented by S_{MAX_OTP}, the current iteration count is represented by j. μ changes with the increase of iteration count, and the formula for calculation is:

$$\mu(j) = \mu_{END}\left(\frac{\mu_{ST}}{\mu_{END}}\right)^{\frac{1}{1+10\,j/S_{MAX\_OTP}}} \tag{19}$$

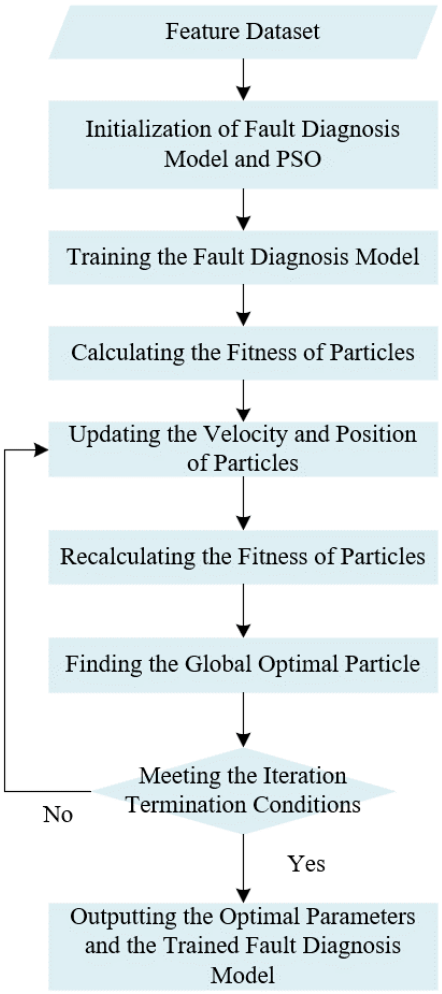

Figure 4. Construction process of the fault diagnosis model.

4. EXPERIMENTAL RESULTS AND ANALYSIS

Fig. 5 compares the permutation entropy values of each IMF component for two sets of signals. The experimental results show that for the two sets of signals (normal signals and signals containing simulated faults), by calculating the permutation entropy values of their respective IMF components, it was found that the permutation entropy values of the IMF components of the fault signals are generally higher than those of the normal signals. Especially in the first six IMF components, this difference is particularly significant. This indicates that fault signals have higher complexity, suggesting the presence of periodic impacts and fault characteristics. From the perspective of permutation entropy, a higher permutation entropy value means the signal has higher unpredictability and complexity, which is consistent with the characteristics of vibration signals under fault conditions. Therefore, by comparing the permutation entropy values of the IMF components of normal and fault signals, key IMF components containing fault information can be effectively identified. Based on this observation, the study chose the first six IMF components for signal reconstruction because these components contain the main fault characteristic information, and also to reduce the complexity and time of computation without losing important information.

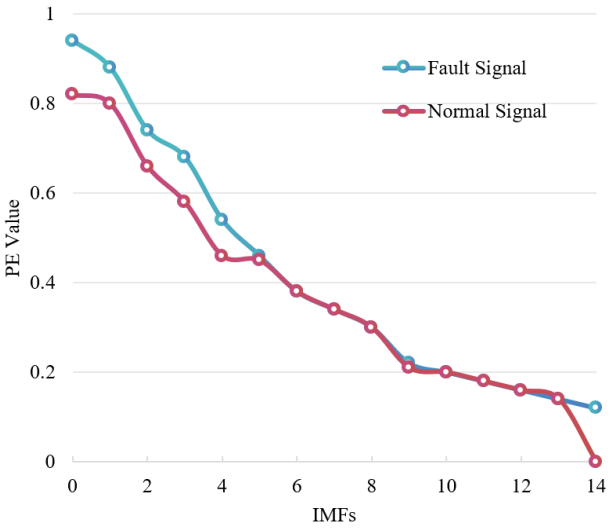

Figure 5: Comparison of permutation entropy values of each IMF component for two sets of signals.

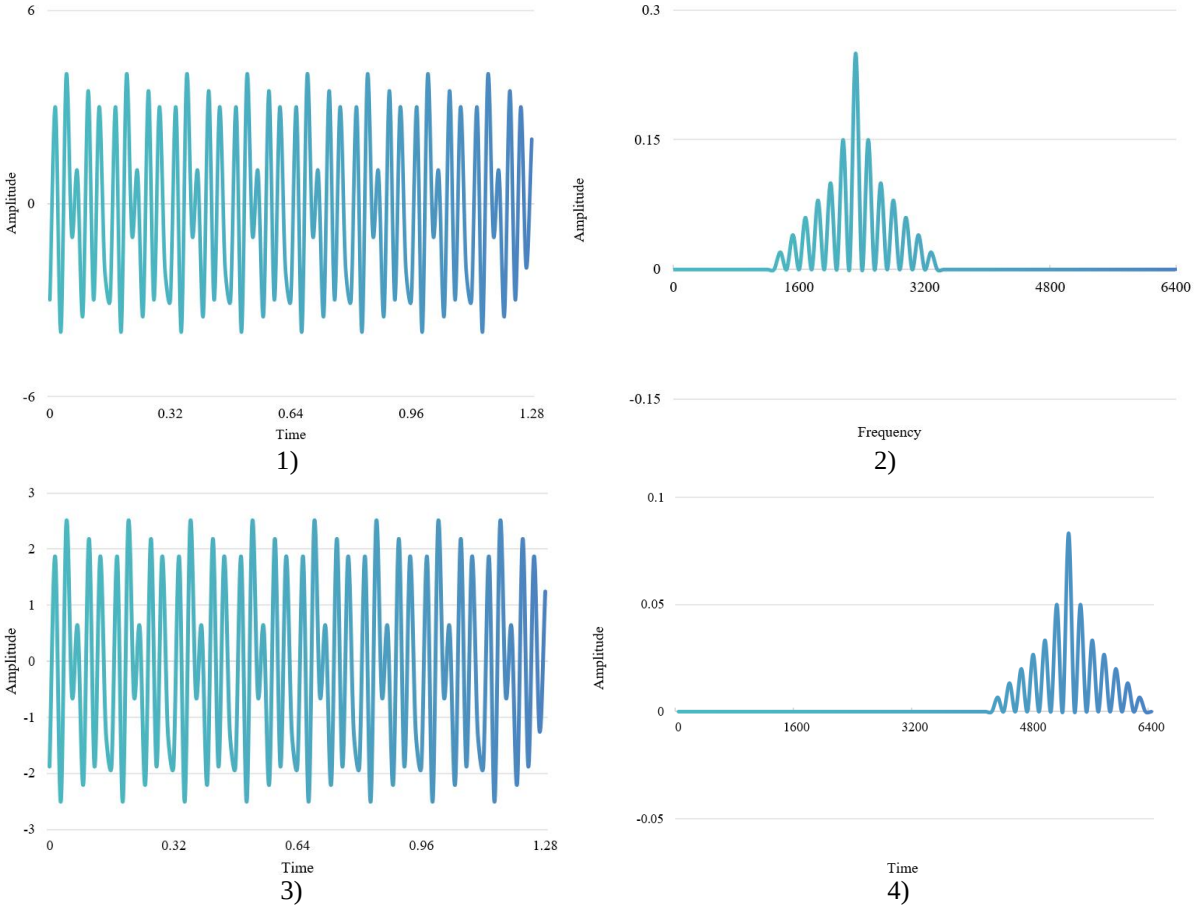

Figure 6: Four decomposition modes of vibration signal from high-efficiency petroleum machinery production system.

Further, by performing VMD on the vibration signal of the high-efficiency petroleum machinery production system, four decomposition modes can be obtained, whose time-domain waveforms and spectrum graphs are shown in Fig. 6. As can be seen from the figure, these modes are the results of signal processing, with each mode reflecting a part of the signal's characteristics. Each decomposition mode has a specific time-domain waveform, indicating that each mode has different vibration characteristics. Spectrum analysis shows that the centre frequencies of these decomposition modes increase in turn, meaning that each mode

corresponds to a different frequency range. At the same time, the amplitude of the corresponding centre frequencies decreases in turn, indicating that the energy of the vibration signal is lower in the high-frequency part. Furthermore, the oscillatory energy of each decomposition mode can be calculated. Since the energy of the low-frequency modes is higher, this may imply that the system's main dynamic response or potential fault characteristics are more likely to appear in the low-frequency range. As the frequency increases, the decrease in energy may indicate that the system's high-frequency response is weaker or the system design naturally attenuates high-frequency vibration energy.

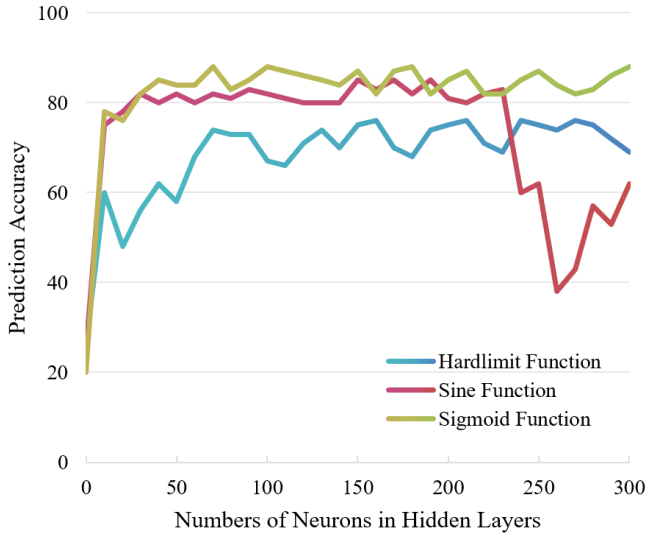

Figure 7: Training set accuracy under different combinations of activation functions and numbers of neurons in hidden layers.

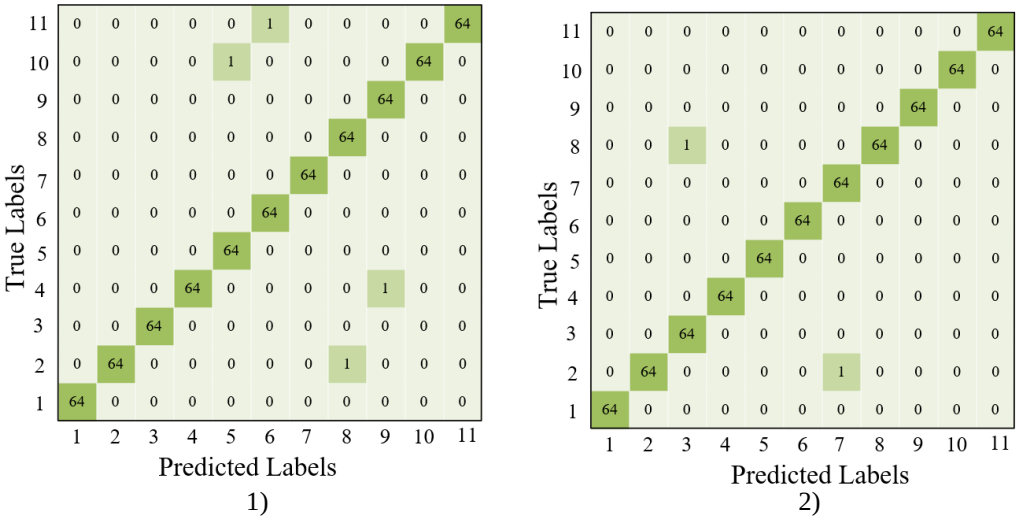

Figure 8: Confusion matrices for the training and testing sets.

This paper further constructs a fault diagnosis prediction simulation model for petroleum machinery production systems based on Adaptive VMD and optimized ELM. Fig. 7 presents the training set accuracy under different combinations of activation functions and numbers of neurons in hidden layers, and Fig. 8 shows the confusion matrices for the training and testing sets. After experimental testing, the combination of the *Sigmoid* activation function and 219 hidden layer neurons was determined to be the best. This combination achieved high accuracy on the training set and realized an accuracy of 99.1 % on the testing set, indicating the model has good generalization ability. Through the confusion matrices, it is observed that there were

4 misjudged samples in the training set and 3 misclassified samples in the testing set. It can be concluded that the simulation model proposed in this paper, based on adaptive VMD and optimized ELM, demonstrates high efficiency and accuracy in fault diagnosis for petroleum machinery production systems. Despite a small number of misjudgements, the overall performance of the model is still very satisfactory.

Table I: Comparison of results for different fault diagnosis prediction simulation models.

Signal processing method	**Fault diagnosis model**	**Training set accuracy** (%)	**Testing set accuracy** (%)
FFT	SVM	78.23	65.24
	BPNN	81.26	77.45
	ELM	81.47	74.21
EDM	SVM	94.56	91.36
	BPNN	96.38	95.87
	ELM	96.78	93.24
VMD	SVM	98.32	92.58
	BPNN	98.15	97.41
	ELM (the proposed model)	97.26	95.32

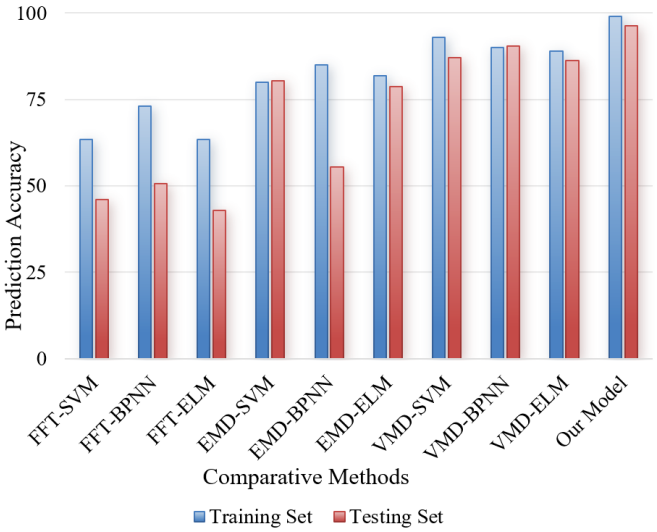

Figure 9: Comparison of simulation results for different fault diagnosis prediction simulation models.

Table I and Fig. 9 present a comparison of training and testing set accuracies for different fault diagnosis prediction simulation models. The accuracy of the model proposed in this paper is 97.26 % on the training set and 95.32 % on the testing set. Although the accuracy on the training set is not the highest, the higher accuracy on the testing set indicates the model has good generalization capability. The accuracy on the testing set is a key indicator of model performance, as it reflects the model's performance on unseen data. The testing set accuracy of the proposed model is higher than that of other combinations, further proving the model's effectiveness. This model combines the effective processing capability of VMD for nonlinear and non-stationary signals with the fast-learning performance of ELM, enhancing the fault diagnosis accuracy through optimization algorithms. The testing set accuracy of this model is superior to similar VMD-based SVM and BPNN models, indicating that the optimized ELM better adapts to features extracted by VMD, thereby achieving better performance in fault diagnosis tasks. It can be concluded that the simulation model proposed in this paper, based on adaptive VMD and optimized ELM, demonstrates superior performance in fault diagnosis

prediction tasks for petroleum machinery production systems compared to other methods and model combinations. The high testing set accuracy reveals its strong generalization capability, indicating that the model not only performs well during the training phase but more importantly maintains high accuracy when facing new data, which is crucial for fault prediction and diagnosis in practical applications.

5. CONCLUSION

This paper proposed a new method for performance evaluation and fault prediction and simulation study of high-efficiency petroleum machinery production systems. Initially, this paper utilized the CEEMD and permutation entropy methods to process the vibration signals of petroleum machinery. CEEMD, as an advanced signal processing technique, allowing for the more accurate separation of IMFs from complex signals, while permutation entropy, as a nonlinear dynamics feature extraction method, was used to capture the complexity and dynamic changes in the signal. By integrating adaptive VMD and optimized ELM, this paper constructed an efficient fault diagnosis prediction model. VMD was used to further extract signal features, and the optimized ELM served as a classifier, with optimization algorithms enhancing learning efficiency and fault diagnosis accuracy.

The experimental section provided a comparison of the permutation entropy values of IMF components for two sets of signals, revealing the characteristics and changes in the vibration signals of high-efficiency petroleum machinery production systems. By testing combinations of different activation functions and numbers of neurons in hidden layers, the experiment explored the impact of ELM model configurations on training set accuracy and presented the classification effects of the training and testing sets in the form of confusion matrices. This paper verified the effectiveness of the proposed model by comparing the results of different fault diagnosis prediction simulation models. The results show that the model combining adaptive VMD and optimized ELM exhibits high accuracy and good generalization capability on the testing set, outperforming other model combinations.

From the comprehensive study content and experimental results, it can be concluded that the simulation model proposed in this paper, based on CEEMD, permutation entropy, adaptive VMD, and optimized ELM, provides an efficient and reliable method for performance evaluation and fault diagnosis of petroleum machinery production systems. This method not only accurately captures the intrinsic features and dynamic changes in vibration signals but also significantly improves the accuracy and efficiency of fault diagnosis through precise model configuration and optimization. The practical application value of this method lies in its significant guidance for fault prevention and maintenance of petroleum machinery production systems, helping to enhance production safety and efficiency while reducing potential operational risks.

REFERENCES

[1] Nandakumar, V.; Shivapriya, S.; Thankan, S. (2024). Utility of fluid inclusion paleo-temperature in petroleum system modelling: a case study from western offshore, India, *Energy Geoscience*, Vol. 5, No. 2, Paper 100256, 19 pages, doi:10.1016/j.engeos.2023.100256

[2] Herrera-Franco, G.; Montalván-Burbano, N.; Mora-Frank, C.; Moreno-Alcívar, L. (2021). Research in petroleum and environment: a bibliometric analysis in South America, *International Journal of Sustainable Development and Planning*, Vol. 16, No. 6, 1109-1116, doi:10.18280/ijsdp.160612

[3] Straka, M.; Sofranko, M.; Glova Vegsoova, O.; Kovalcik, J. (2022). Simulation of homogeneous production processes, *International Journal of Simulation Modelling*, Vol. 21, No. 2, 214-225, doi:10.2507/IJSIMM21-2-597

[4] Sun, F.; Sun, C.; Dong, H.; Jin, J.; Li, Y. (2021). Research on the intelligent information platform construction of petroleum engineering, *2021 3rd International Conference on Artificial Intelligence and Advanced Manufacture*, 525-529, doi:10.1145/3495018.3495112
[5] Zhao, H.; Du, H.; Peng, Z.; Zhang, T. (2023). Thermodynamic performance analysis of a novel energy storage system consist of asymmetric PEMEC and SOFC combined cycle, *Energy Conversion and Management*, Vol. 286, Paper 117077, 14 pages, doi:10.1016/j.enconman.2023.117077
[6] Cui, Y. (2021). Vision system of welding robot based on DA-XGboost algorithm, *2nd International Conference on Distributed Sensing and Intelligent Systems*, 139-149, doi:10.1049/icp.2021.2670
[7] Ohkawa, S.; Yun, S.; Hibiya, T.; Nishimura, H. (2019). A new process to develop a hydraulic system adapted to biodegradable hydraulic oil for construction machinery: case study integrating component analyses and SysML description in failure analyses, *Synthesiology*, Vol. 12, No. 2, 57-74, doi:10.5571/syntheng.12.2_56
[8] Ettl, J.; Bernhardt, H.; Huber, G.; Thuneke, K.; Remmele, E.; Emberger, P. (2020). Evaluation of pure rapeseed oil as a renewable fuel for agricultural machinery based on emission characteristics and long-term operation behaviour of a fleet of 18 tractors, *SN Applied Sciences*, Vol. 2, Paper 1711, 16 pages, doi:10.1007/s42452-020-03490-8
[9] Siddiqui, M.; Pal, S. K.; Dewangan, N.; Chattopadhyaya, S.; Sharma, S.; Nekoonam, S.; Issakhov, A. (2021). Sludge formation analysis in hydraulic oil of load haul dumper 811MK V machine running at elevated temperatures for bioenergy applications, *International Journal of Chemical Engineering*, Vol. 2021, Paper 4331809, 14 pages, doi:10.1155/2021/4331809
[10] Dalfi, H.; Al-Obaidi, A.; Tariq, A.; Razzaq, H.; Rafiee, R. (2024). Optimization of the mechanical performance and damage failure characteristics of laminated composites based on fiber orientation, *Frontiers of Structural and Civil Engineering*, Vol. 17, No. 9, 1357-1369, doi:10.1007/s11709-023-0996-4
[11] Idumah, C. I. (2023). MXene polymeric nanoarchitectures mechanical, deformation, and failure mechanism: a review, *Polymer-Plastics Technology and Materials*, Vol. 62, No. 4, 443-466, doi:10.1080/25740881.2022.2114365
[12] Zhang, X.; Yu, L.; Wang, M.; Yang, H. (2024). Mechanical response and failure characteristics of tunnels subjected to reverse faulting with nonuniform displacement: theoretical and numerical investigation, *Engineering Failure Analysis*, Vol. 156, Paper 107809, 26 pages, doi:10.1016/j.engfailanal.2023.107809
[13] Yu, L.; Liu, G.; Wang, W.; Hamada, H.; Yang, Y. (2023). Mechanical failure analysis of pultrusion glass fiber pipe based on acoustic emission technology, *Polymer Composites*, Vol. 44, No. 4, 2196-2204, doi:10.1002/pc.27236
[14] Wang, Y.; Jagota, V.; Makhatha, M. E.; Kumar, P. (2022). Vibration signal acquisition and computer simulation detection of mechanical equipment failure, *Nonlinear Engineering*, Vol. 11, No. 1, 207-214, doi:10.1515/nleng-2022-0026
[15] Wu, S. (2023). Vibration signal analysis of complex mechanical systems and early wear detection and forecasting for gears, *Traitement du Signal*, Vol. 40, No. 5, 2101-2109, doi:10.18280/ts.400527
[16] Cam, S.; Oguztuzun, H.; Yilmaz, L. (2022). Hypothesis-driven simulation experiments with an extension to SED-ML, *International Journal of Simulation Modelling*, Vol. 21, No. 1, 17-28, doi:10.2507/IJSIMM21-1-583
[17] Yang, Y.; Zhang, Z.; Xu, L.; Yao, G. (2022). Mechanical performance and failure mode research on the braced frame joint of tower cranes in high-rise building construction, *Frontiers in Materials*, Vol. 9, Paper 824693, 13 pages, doi:10.3389/fmats.2022.824693